

Bayesian Optimization of a Wearable Assistive Device Using an Estimator Stopping Process

A thesis presented

by

Charles Liu

to

Institute of Applied Computational Science

in partial fulfillment of the requirements

for the degree of

Master of Engineering

in the subject of

Computational Science & Engineering

Harvard University

Cambridge, Massachusetts

May 2018

© 2018 Charles Liu

All rights reserved.

Thesis Advisor:

Professor Scott Kuindersma

Author:

Charles Liu

Bayesian Optimization of a Wearable Assistive Device Using an Estimator Stopping Process

Abstract

Recent *human-in-the-loop* (HIL) optimization studies using wearable devices have shown an improved average metabolic reduction by optimizing control parameters online during short-duration experiments. However, the coupling of slow metabolic dynamics, high measurement noise, and hard experimental time constraints creates significant practical challenges for scaling optimization methods to more expressive control strategies. Prior work on applying gradient descent and Bayesian optimization methods to perform HIL optimization have decoupled the estimation and parameter selection problems, which leads to fixed estimation intervals and imposes a hard limit on the number of parameter evaluations possible in a given time budget. In this work, a different approach is taken that couples estimation and parameter selection, allowing the algorithm to spend less time refining the metabolic estimates for parameters that are unlikely to improve performance over the best values observed so far. We represent this early stopping mechanism with two different models that are incorporated in a standard Bayesian optimization scheme using an unscented Kalman filter for estimating metabolic rate. Performance is analyzed in several numerical examples and in pilot experiments with two human subjects optimizing 6 free control parameters of a hip soft exosuit.

Contents

Abstract	iii
Acknowledgments	x
Introduction	1
1 Bayesian Optimization	4
1.1 Gaussian Processes	4
1.2 GP Regression and Acquisition Functions	5
1.3 Hyperparameter Optimization and Student-t Noise Model	7
1.4 Implementation	8
2 Metabolic Cost Estimation	10
2.1 Instantaneous Energetic Cost	10
2.2 Parameter Estimation	11
2.3 UKF Covariance Parameters	12
2.4 Testing and Future Improvements	13
3 Measurement Stopping Algorithms	17
3.1 Stopping Problem	17
3.2 σ -scaled Offset	18
3.3 Gittins Index	19
3.4 Adaptive Thresholds	21
3.5 Simulations	21
4 Results	23
4.1 Experimental Protocol	23
4.2 Experimental Subjects	25
4.3 Results	26
4.4 Conclusions	27
References	29

Appendix A Bayesian Optimization	33
Appendix B Unscented Kalman Filter	35
Appendix C Optimal Stopping Time Derivation	37

List of Tables

2.1	Tuning Parameters for metabolic estimator	13
3.1	Setup of finite horizon stopping problem	17
3.2	Optimization functions for simulations	22
4.1	6 parameters for providing a force profile	23
4.2	Subject Trial Summary	27

List of Figures

1.1	Sample GP Regression of a function using squared exponential and Matérn kernels.	6
1.2	Gaussian MAP estimate vs. Student-t Gibbs Sampler. Data points added with Gaussian noise including some outliers with very high variance.	9
2.1	Sample estimation process for instantaneous energetic cost.	11
2.2	With a true instantaneous energetic cost at 350 and prior at 300, keeping all other parameters constant, the effect of using various P_w values on measurement variance.	14
2.3	Tuned UKF Estimator over previously collected data. Accuracy assessed over partial data.	15
2.4	Tuned UKF Estimator shows different levels of noise during optimization studies on different subjects.	16
4.1	Experimental setup. Assistance parameters for the soft exosuit were optimized on-line. Respiratory device measured respiratory rate to estimate metabolic cost for a given condition with a covariance. In the optimization computer, the Gittins process determined when to stop sampling and Bayesian optimization was used to select a next parameter set. The parameters were sent to the real-time computer (speedgoat) to generate a force trajectory. Then, the actuator provided a force to a subject through a bowden cables.	26
4.2	Diagram of Bandit Process	27
4.3	Force profiles of the two subjects	28

A.1 Demonstration of the effect of fixing measurement noise for each data point. Using the same data from Figure 1.2, the top graph shows the same MCMC graph that infers the noise hyperparameters with the highest likelihood. In the bottom graph, the noise parameters are fixed and inversely proportional to the true accuracy - in effect telling the GP that the outliers are the correct values. This may arise in situations where a minimum is found (measured for the full duration, resulting variance is relatively low) and many nearby points are subsequently sampled and stopped early (resulting variances are very high).	33
A.2 Four Iterations of Bayesian Optimization	34

List of Algorithms

1	Bayesian Optimization Outline	7
2	Determining threshold levels for either model based on subject's exploration data. With the σ -offset, a higher threshold is more risk averse, while with the Gittins model a lower is.	22

Acknowledgments

I am very grateful to Scott Kuindersma for being an incredible advisor. It has been a privilege to be his student and I appreciate his guidance, patience, and immense knowledge in helping me throughout the course of my study. It has also been a pleasure to work with Myunghee Kim, who was integral to the work in this thesis. Her wealth of experience in the field as well as overseeing the various levels of development was instrumental. I'd also like to thank Professor Conor Walsh, his lab and the Wyss staff, in particular Nikos Karavas, Sangjun Lee, Jinsoo Kim, Chih-Kang Chang, Asa Eckert-Erdheim, Maria Athanassiu, Brice Mikala Iwangou, Nicolas Menard, and Sarah Sullivan. This work would not have been possible without the hard work of everyone involved from the design and fabrication of the exosuit to the development of the controllers. Finally, I thank my parents, my friends, and the rest of my family for their amazing support.

Introduction

Wearable robotic devices are intended as a means to augment human economy, strength, and endurance. Over the past decade, a number of devices have been developed for reducing the metabolic cost of walking for able-bodied individuals (Malcolm *et al.*, 2013; Mooney and Herr., 2016; Caputo and Collins, 2014; Panizzolo *et al.*, 2016a). With tethered and portable hardware platforms having advanced considerably (Malcolm *et al.*, 2013; Lee *et al.*; Panizzolo *et al.*, 2016b), it is now possible to accurately control settings such as the timing and magnitude of the delivered torque (Malcolm *et al.*, 2013; Collins *et al.*, 2015; Ding *et al.*, 2017; Kim and Collins, 2015, 2017; Lee *et al.*, 2016). Increased attention has been directed towards how control strategy and control parameters influence overall system performance (Caputo and Collins, 2014; Kim and Collins, 2015, 2017; Quinlivan *et al.*, 2017). Traditionally, control parameters have been tuned manually by researchers with expert knowledge on both the device and biomechanics of human walking or through exploring the parameter space in a systematic sweep (Caputo *et al.*, 2015; Quinlivan *et al.*, 2017). However, despite these efforts, several studies have shown significant inter-subject variability in the observed metabolic benefit for a fixed parameter setting (Quesada *et al.*, 2016). Being able to automatically recover the optimal parameter setting on an individual basis is therefore a fundamental component in designing effective wearable robotic devices.

Recently, several groups have explored different formulations of *human-in-the-loop* (HIL) optimization that offer the possibility to avoid conventional exhaustive search (Koller *et al.*, 2016; Zhang *et al.*, 2017; Ding *et al.*, 2018; Kim *et al.*, 2017). These studies use instantaneous energetic cost (Selinger and Donelan., 2014), an estimation of steady-state metabolic cost, as

an objective measurement for automatically optimizing parameter settings (Koller *et al.*, 2016; Felt *et al.*, 2015; Zhang *et al.*, 2017; Ding *et al.*, 2018). Previous research has applied this HIL optimization approach to find optimal onset actuation timing of a bilateral pneumatic ankle exoskeleton by automatically adjusting a single control parameter (Koller *et al.*, 2016). A recent study with an ankle exoskeleton (Zhang *et al.*, 2017) and hip exosuit (Ding *et al.*, 2018) showed the potential to achieve larger metabolic benefits by simultaneously optimizing multiple parameters using *Bayesian optimization*.

Motivation

Bayesian optimization is a sequential optimization strategy that has been used in a variety of applications from hyperparameter tuning for machine learning algorithms (Snoek *et al.*, 2012; Mahendran *et al.*, 2012) to portfolio allocation (Brochu *et al.*, 2010) and experimental design (Brochu and De Freitas, 2010). As it is a general framework to optimize noisy black box functions, many variations have been introduced to account for different use cases. In particular, an area of interest has been in tackling the noisiness of data samples (Rue *et al.*, 2009; Nogueira *et al.*, 2016; Assael *et al.*, 2014) and the myopia of the algorithm (Lam *et al.*, 2016; González *et al.*, 2015).

The algorithm is typically framed in the context of an iteration budget, abstracting away the actual data sampling process. However, in the HIL problem there is a limited time constraint rather than an iteration constraint, and data acquisition exhibits a direct tradeoff between noisiness and elapsed time. In previous studies, a fixed observation window was used for every parameter evaluation, effectively reducing the time constraint to an iteration constraint. Unfortunately, this means spending valuable time measuring parameter settings that are unlikely to improve upon the best value observed so far.

Summary of contributions

The main contribution of this work is to introduce a stopping problem within a given evaluation of Bayesian optimization. Rather than having a fixed observation window, a stopping rule is determined after every respiratory measurement to maximize the time spent evaluating promising parameter settings. To determine the optimal stopping time, a metabolic cost estimator is also developed to provide a probability distribution of the instantaneous energetic cost after every measurement.

Outline

Chapter 1 gives background information on Bayesian optimization and Gaussian processes. Chapter 2 presents the metabolic estimator and its robustness under various levels of noise. Initial experimental data is provided and future work on the estimator is discussed. Chapter 3 introduces two algorithms for determining the optimal stopping point within an iteration of Bayesian Optimization. Simulations of various optimization functions are provided using the two algorithms under different scenarios. Chapter 4 provides results from an experimental protocol using one of the algorithms. Finally, we conclude this thesis with a discussion of future work.

Chapter 1

Bayesian Optimization

1.1 Gaussian Processes

Given a parameter space $\mathbb{X} \subset \mathbb{R}^m$ and an unknown, noisy energetic cost function f that is expensive to evaluate, we aim to find the solution to the minimization problem

$$x^* = \arg \min_{x \in \mathbb{X}} f(x), \quad (1.1)$$

by iteratively choosing points to evaluate until a finite time constraint is met. Bayesian optimization, our sequential design strategy, computes a posterior distribution on possible objective functions given all previous evaluations and optimizes an acquisition function on this distribution to globally select the next value of x to evaluate, typically in a way that carefully balances exploration and exploitation. The distribution over f is modeled as a Gaussian process (Rasmussen, 2006) \mathbb{G} ,

$$f \sim \mathbb{G}(\mu, \kappa), \quad (1.2)$$

where $\mu : \mathbb{X} \rightarrow \mathbb{R}$ is a mean function typically set to zero, and $\kappa : \mathbb{X} \times \mathbb{X} \rightarrow \mathbb{R}$ is a covariance kernel that characterizes the correlation between different points in the domain. The most

common example for the covariance kernel is the squared exponential

$$\kappa(x_i, x_j | \theta) = \sigma_\theta^2 \exp\left(-\frac{1}{2} d^2\left(\frac{x_i}{l}, \frac{x_j}{l}\right)\right), \quad (1.3)$$

with parameters $\theta = [\sigma_\theta^2, l]$ where l is either a scalar or vector of dimension m . The Matérn covariance kernel is a more generalized form of the squared exponential, defined as

$$\kappa(x_i, x_j | \theta) = \sigma_\theta^2 \frac{2^{1-\nu}}{\Gamma(\nu)} (\sqrt{2\nu} d\left(\frac{x_i}{l}, \frac{x_j}{l}\right))^\nu K_\nu(\sqrt{2\nu} d\left(\frac{x_i}{l}, \frac{x_j}{l}\right)) \quad (1.4)$$

with $\theta = [\sigma_\theta^2, l, \nu]$ and K_ν is a modified Bessel function.

1.2 GP Regression and Acquisition Functions

By definition of a GP, any collection of points forms a multivariate normal distribution defined by μ and κ . Under this assumption, a posterior distribution given a set of training samples can be solved analytically. Formally, given some training samples $S = \{(x_i, y_i)\}_{i=1}^n$, and assuming each sample follows a Gaussian noise model $y_i \sim f(x_i) + \mathcal{N}(0, \sigma_n^2)$, the posterior distribution at x is Gaussian with mean $\bar{\mu}(x)$ and variance $\bar{\sigma}^2(x)$ evaluated as

$$\bar{\mu}(x) = K(X, x)^T [K(X, X) + \sigma_n^2 I]^{-1} Y \quad (1.5)$$

$$\bar{\sigma}^2(x) = \kappa(x, x | \theta) - K(X, x)^T [K(X, X) + \sigma_n^2 I]^{-1} K(X, x) \quad (1.6)$$

$$K(X, x)_i = \kappa(x_i, x | \theta)$$

$$K(X, X)_{ij} = \kappa(x_i, x_j | \theta),$$

where $X = \{x_i\}_{i=1}^n$ and $Y = \{y_i\}_{i=1}^n$.

Given a distribution at point x , an acquisition function captures how attractive that point is to sample next. A common choice of acquisition function is Expected Improvement (EI), which returns the expected reduction in cost over the best parameters observed so far. For

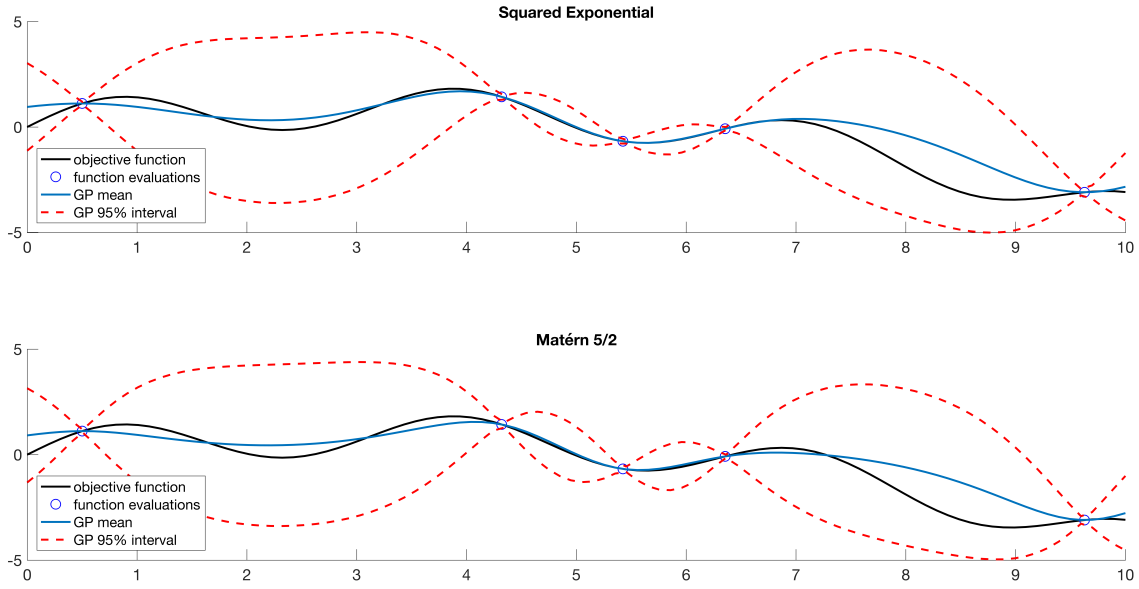


Figure 1.1: Sample GP Regression of a function using squared exponential and Matérn kernels.

the given GP model, EI can be computed in closed form:

$$\begin{aligned}
 EI(x|S) &= \int_{\infty}^{\infty} \max(0, y^* - y) p(y|x) dy \\
 &= z\bar{\sigma}(x)\Phi(z) + \bar{\sigma}(x)\phi(z) \\
 z &= \frac{y^* - \bar{\mu}(x) + \xi}{\bar{\sigma}(x)},
 \end{aligned} \tag{1.7}$$

where y^* is the best value observed so far and ξ is a scaling parameter to adjust the tradeoff between exploration-exploitation (Lizotte, 2008). The next point to evaluate is then chosen as $x^* = \arg \max_x EI(x|S)$. Figure A.2 shows a few iterations of Bayesian Optimization on a sample function.

The choice of y^* can be defined as the minimum observed value so far, the minimum $\bar{\mu}(x)$ under the current GP model over all previous observations, or some biased version thereof (Lizotte, 2008).

```

Objective Function  $F(x)$ 
Acquisition Function  $g(\mu, \sigma^2)$ 
Specify Exploration Points  $\mathbb{E} = \{e_1, e_2, \dots, e_n\}$ 
Training Samples  $S$ 
for  $i = 1$  to  $n$ 
     $S = S \cup \{e_i, F(e_i)\}$ 
end
while  $t < T$ 
    Update GP Hyperparameters  $\theta$ 
    Given  $f(x|\theta, S) \sim \mathcal{N}(\mu_x, \sigma_x^2)$ ,
     $x^* = \arg \max_{x \in \mathbb{X}} g(\mu_x, \sigma_x^2)$ 
     $S = S \cup \{x^*, f(x^*)\}$ 
end

```

Algorithm 1: Bayesian Optimization Outline

1.3 Hyperparameter Optimization and Student-t Noise Model

The values of the hyperparameters in the kernel function are critical to determining the posterior distribution. Typically, these hyperparameters are tuned to sampled points with a maximum a posteriori (MAP) point estimate (Snoek *et al.*, 2012; Jarno Vanhatalo and Vehtari, 2013). Specifically, assuming our Gaussian noise model we have an analytical solution

$$\begin{aligned}
& \arg \max_{\theta, \sigma_n^2} \log P(S|\theta, \sigma_n^2) + \log P(\theta, \sigma_n^2) \\
&= \log \int p(Y|f, \sigma_n^2) p(f|X, \theta) df + \log P(\theta, \sigma_n^2) \\
&= -\frac{n}{2} \log(2\pi) - \frac{1}{2} \log(K(X, X) + \sigma_n^2 I) - \frac{1}{2} Y^T (K(X, X) + \sigma_n^2 I)^{-1} Y + \log P(\theta, \sigma_n^2)
\end{aligned} \tag{1.8}$$

Instead of using a single point estimate, a full Bayesian approach would involve marginalizing out the hyperparameters through an MCMC approximation. This would be particularly beneficial in the case that the posterior is multi-modal or sensitive to small changes in hyperparameter values. Many sampling approaches have been proposed, and we refer the reader to (Barber *et al.*, 2011, Chapter 14) for a summary.

The MCMC approach is also used in more complex noise models whose posterior distribution and marginal likelihood are no longer analytically tractable. Vanhatalo *et al.*

(2009); Jylänki *et al.* (2011) developed a more robust, heteroscedastic noise model based on the Student-t distribution to handle occurrences of large outliers in the collected data. The noise distribution follows

$$p(y_i|f, \sigma_i^2, \nu) = \frac{\Gamma(\frac{\nu+1}{2})}{\Gamma(\frac{\nu}{2})\sqrt{\nu\pi\sigma_i^2}}(1 + \frac{(y - f)^2}{\nu\sigma_i^2})^{-\frac{(\nu+1)}{2}} \quad (1.9)$$

where ν is a degrees of freedom hyperparameter. A Gibbs sampler can be performed through a hierarchical model

$$\begin{aligned} y_i|f &\sim \mathcal{N}(f, V) \\ V &\sim \text{Inv-}\chi^2(\nu, \sigma_i^2), \end{aligned} \quad (1.10)$$

with θ alternately sampled according to the Gaussian Process. Figure 1.2 shows a comparison of the robust Student-t noise with the standard Gaussian noise. The majority of the data points exhibit low variances, while some extreme outliers are also produced. While the Gaussian noise model treats each data point equally, the Student-t model is able to reach a noise distribution that effectively matches the underlying function.

1.4 Implementation

There are a number of implementation choices relevant to HIL optimization. While the MCMC approach has shown to be more robust, GP regression scales linearly with the number of samples. As such, an accurate optimization of the acquisition function can take on the order of minutes. However, once a stopping condition is met the next parameter setting must immediately be communicated to the wearable device. In our implementation, we start a sampler as soon as a new parameter evaluation starts. When the stopping condition is met, if the MCMC has completed optimizing EI we use the returned parameter setting to sample next. Otherwise, we default to the MAP estimate. There is then a tradeoff of the standard MAP estimate with a more robust MCMC sampler that uses one less training sample.

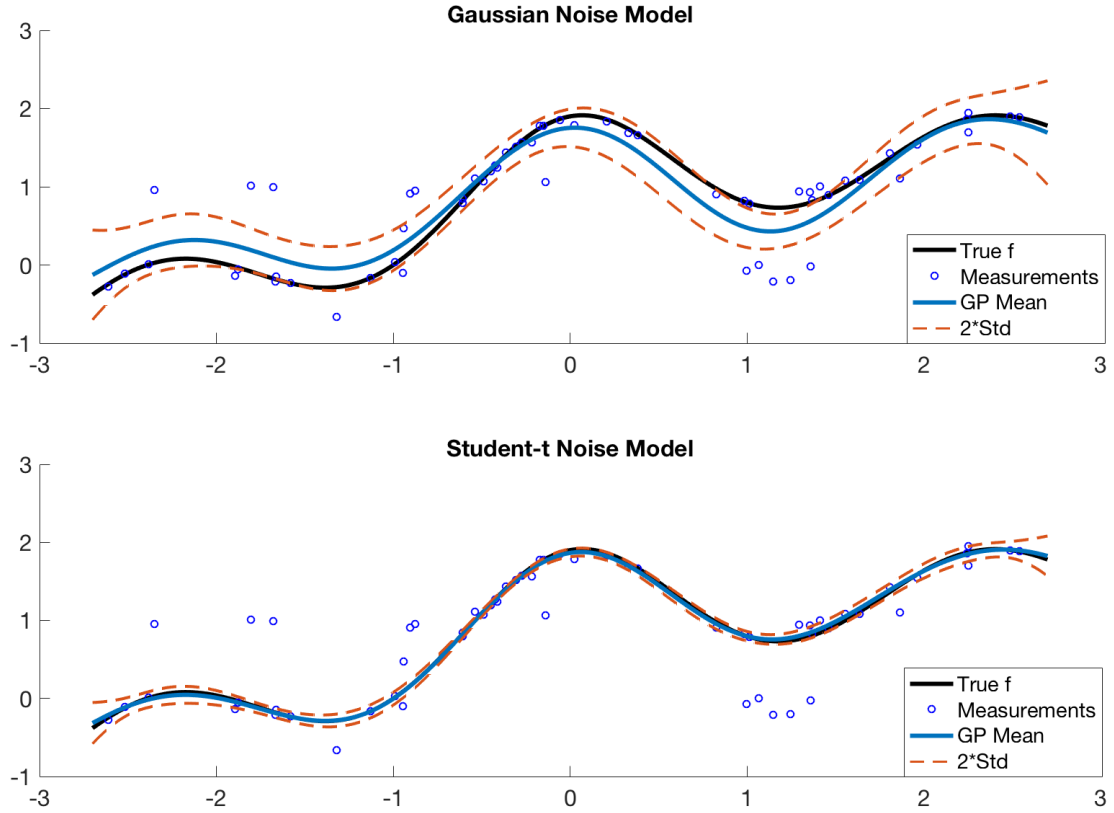


Figure 1.2: Gaussian MAP estimate vs. Student-t Gibbs Sampler. Data points added with Gaussian noise including some outliers with very high variance.

As Chapter 2 will discuss, the returned metabolic estimates have an associated variance; earlier stopping points exhibit a higher variance representing greater uncertainty for the estimated cost. As a result, the GP mean may incorrectly inflate the best observed value if a number of parameter settings nearby are stopped early (see MAP estimate in Figure 1.2 for $x \in (-2, -1)$). For this reason in the Expected Improvement function we treat y^* as the best observed value so far, not the regression mean. We also fix the noise hyperparameters in the MCMC method proportional to the estimator variances, effectively giving more weight to the observations measured the full duration. Figure A.1 gives an example of the effect of fixed noise hyperparameters on the GP.

Chapter 2

Metabolic Cost Estimation

2.1 Instantaneous Energetic Cost

The instantaneous energetic cost, our objective function, is estimated through continuous breath measurements over a lengthy duration of time. Brockway (1987) developed a formula for converting CO_2 and O_2 measurements into a metabolic cost, which is then fit into a first-order dynamical model. Given the noisiness of respiratory measurements, previous studies (Felt *et al.*, 2015; Selinger and Donelan., 2014) allowed three minutes while subjects reached a steady state before measuring for an additional three minutes to estimate an instantaneous energetic cost. In a previous Bayesian optimization study (Ding *et al.*, 2018), each iteration used a fixed two minutes of respiratory measurements.

Rather than requiring a fixed time interval for each evaluation, we aim to ascertain an accurate estimate only for promising parameter settings while stopping early for those that are unlikely to improve upon the best settings found so far. To make that determination, an online estimator for instantaneous energetic cost was developed using the metabolic cost model

$$m_t(c_0, c, \tau_0, \tau) = c(1 - e^{\frac{-t}{\tau}}) + c_0 e^{\frac{-t}{\tau_0}}, \quad (2.1)$$

where t is the total measurement time in seconds and τ_0, τ are time constants characterizing

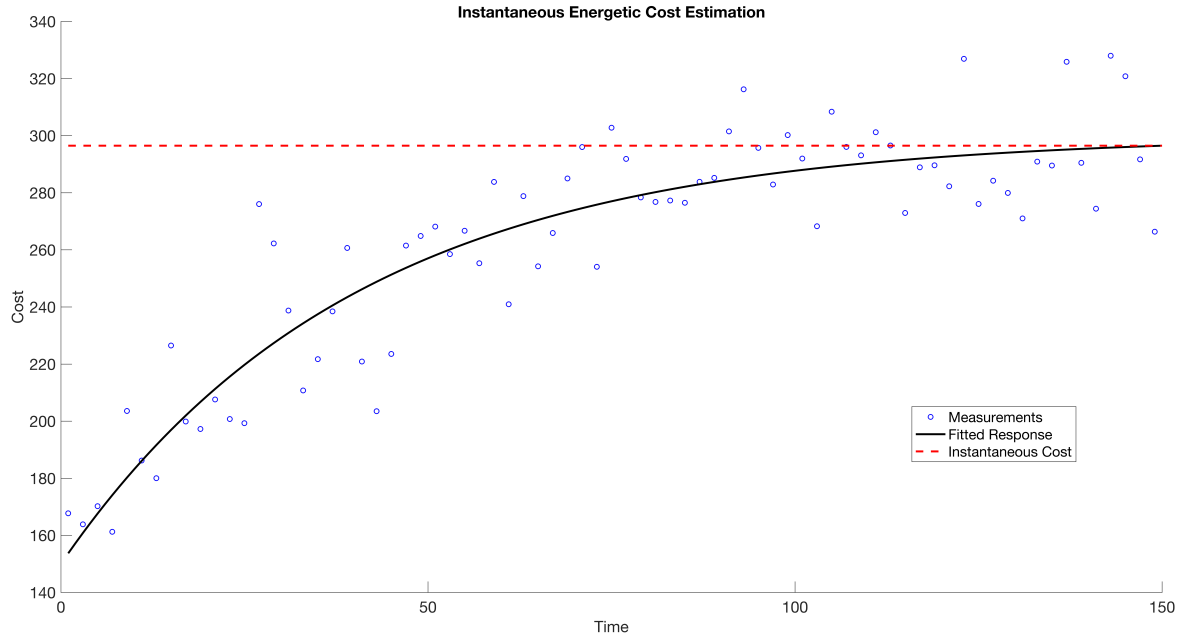


Figure 2.1: Sample estimation process for instantaneous energetic cost.

the rate of change for the initial cost c_0 and the instantaneous energetic cost c respectively.

2.2 Parameter Estimation

The time and cost parameters are estimated through an Unscented Kalman Filter (Julier, 1997). Kalman filters are applied to discrete time systems of the form

$$\begin{aligned} x(t+1) &= F(x(t), v(t), t) \\ z(t) &= H(x(t), w(t), t), \end{aligned} \tag{2.2}$$

where $x(t)$ represents the unobserved state of the system, $z(t)$ the observed measurement, and zero-mean Gaussian vectors $v(t)$ for process disturbances or modeling errors and $w(t)$ for measurement noise.

First, a prediction is made for the state of the system after one timestep. Let $\hat{x}(t|t-1)$ represent the estimate for $x(t)$ using measurements $Z(t-1) = [z(1), z(2), \dots, z(t-1)]$ and

$P_x(t|t-1)$ the covariance for the estimate. The prediction step aims to calculate

$$\begin{aligned}\hat{x}(t|t-1) &= \mathbb{E}[F(x(t-1), v(t-1), t-1)|\mathbb{Z}(t-1)] \\ P_x(t|t-1) &= \mathbb{E}[\{\hat{x}(t|t-1) - x(t)\}\{\hat{x}(t|t-1) - x(t)\}^T|\mathbb{Z}(t-1)]\end{aligned}\tag{2.3}$$

The prediction is then reconciled with the observed measurement through a minimum mean-squared estimate $\hat{x}(t)$ and covariance $P_x(t)$ according to the following equations

$$\begin{aligned}\hat{x}(t) &= \hat{x}(t|t-1) + K\mathbb{E}[y] \\ P_x(t) &= P_x(t|t-1) - KP_y(t|t-1)K^T \\ K &= P_{xy}(t|t-1)P_y^{-1}(t|t-1) \\ y &= z(t) - H(\hat{x}(t|t-1), w(t), t)\end{aligned}\tag{2.4}$$

The underlying requirement for these equations is an accurate propagation of the first two moments of $x(t)$ and $z(t)$. As such, Gaussian distributions are assumed as they have the least information. When F or H is nonlinear, rather than linearizing the functions with a first order approximation the UKF approximates its probability distribution through an unscented transformation. The complete implementation details for the UKF are outlined in Appendix B.

As we consider τ_0, τ, c, c_0 to be constant parameters, our UKF setup is

$$\begin{aligned}x &= [c_0 \quad c \quad \tau_0 \quad \tau] \\ F(x(t), v(t), t) &= x(t) + v(t) \\ H(x(t), w(t), t) &= m_t(x(t)) + w(t)\end{aligned}\tag{2.5}$$

2.3 UKF Covariance Parameters

The UKF algorithm has covariance parameters P_x for the state estimate, P_w for measurement noise, and P_v for process noise that determine the sensitivity of the state estimate to new measurements. Table 2.1 summarizes the effect of increasing one of these covariance parameters while holding all others constant.

The volatility of the estimator is dependent on the calibration of the covariance parame-

Increase In	Effect On State Estimate
P_x	A higher initial covariance on the state estimate implies higher uncertainty with the state prior. Early observations will have a greater effect on the state update. However, P_x decreases after every state update; observations therefore will have a smaller effect on the state estimate over time
P_w	A higher measurement noise will reduce an observation's effect on the state update. The state will be to slow to move away from the prior, particularly in early observations. P_w also affects P_x on future timesteps, as the covariance is bounded by P_w
P_v	While F is essentially the identity function in the metabolics model as the cost and time parameters are assumed to be constant, P_v encapsulates the error in that model as well as outside disturbances that can't be measured such as fatigue. Increasing P_v can be used to enforce a lower bound on the effect of an observation to the state update

Table 2.1: Tuning Parameters for metabolic estimator

ters with respect to the noise of the measurements. Figure 2.2 shows three estimators: one that underestimates the measurement noise by a factor of 10, one that is exact, and one that overestimates by a factor of 10. Underestimating leads to a higher weight given to the measurement on subsequent state updates, with the volatility initially quite high. As more measurements are taken and P_x decreases, the estimator eventually reaches a steady state. On the other hand, assuming too high a measurement noise will cause the estimator to slowly update towards the true value.

2.4 Testing and Future Improvements

Using previously attained metabolic data, Figure 2.3 shows the raw and noisy measurements taken and the metabolic cost prediction that the model developed in response to a representative participant¹. The bottom plot displays the covariance associated with the cost, beginning with a covariance of 1 and converging at different rates depending upon the

¹Testing carried out by Myunghee Kim

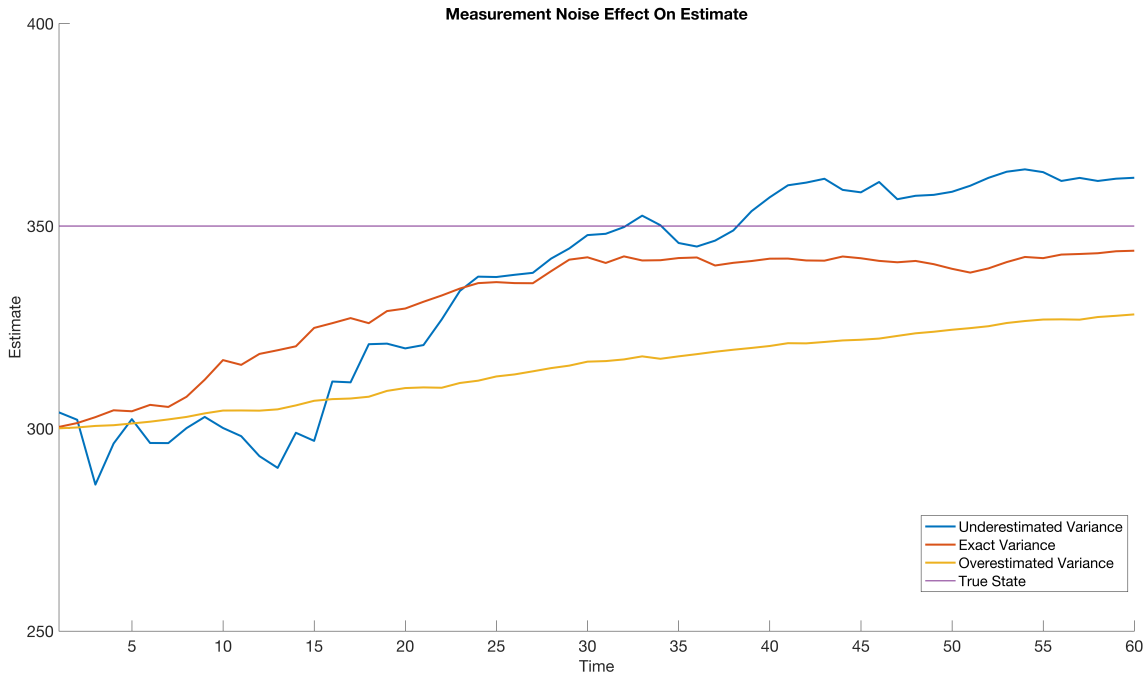
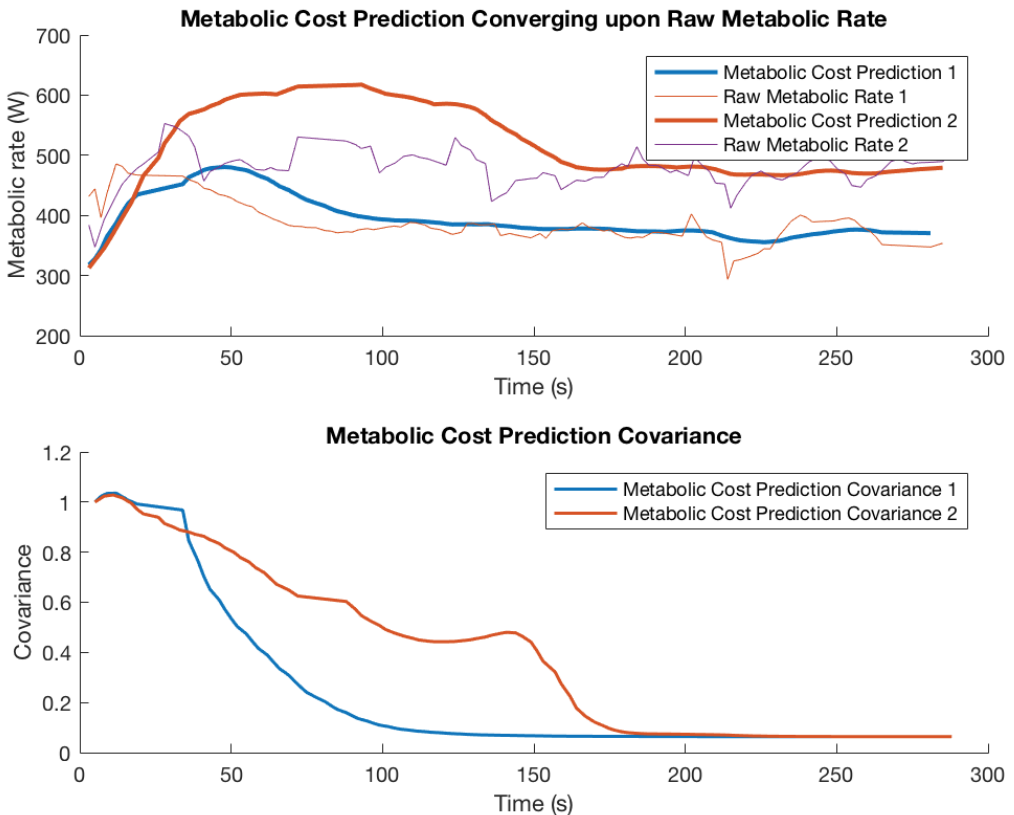


Figure 2.2: With a true instantaneous energetic cost at 350 and prior at 300, keeping all other parameters constant, the effect of using various P_w values on measurement variance.

raw data. When tuned properly, both trials see a relatively smooth rate of convergence of the estimate. With varying amounts of data provided, the accuracy in percent error was calculated by comparing with a "ground truth" value at each termination condition (5 min, 2 min, 1.5 min, 20 breaths, and 30 breaths). This ground truth value is the average of the last two minutes of data, when the subject has reached steady-state.

During trial testing for our optimization methods, the UKF estimator showed various levels of volatility across subjects (Figure 2.4). Future work on the estimator would involve creating a cost function to optimize across the various covariance parameters, as these values should also be subject-specific. The cost function should balance between the smoothness of the estimation curve and eventual convergence to the "true cost". As Bayesian optimization starts with an exploration phase that will measure a specified number of points for the maximum duration, the estimator can then be tuned real-time a posteriori. Without this tuning, the next chapter will go into modeling the stopping problem while taking into account the accuracy of the estimator.



Data Used	Average R^2	Max % Error
Full Trial	0.996	0.977%
2 Minutes	0.984	0.984%
1.5 Minutes	0.973	0.973%
30 Breaths	0.966	3.113%
20 Breaths	0.890	5.767%

Figure 2.3: Tuned UKF Estimator over previously collected data. Accuracy assessed over partial data.

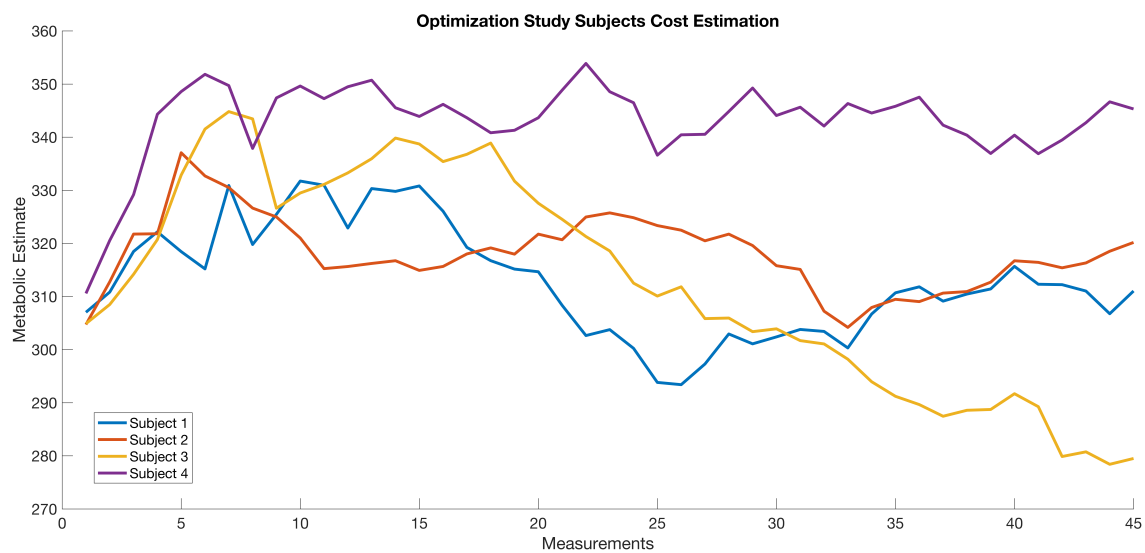


Figure 2.4: Tuned UKF Estimator shows different levels of noise during optimization studies on different subjects.

Chapter 3

Measurement Stopping Algorithms

3.1 Stopping Problem

With an estimate and associated variance for the instantaneous energetic cost, the determination for when to stop measuring is known as a finite-horizon stopping problem. Formally, the stopping problem is defined with

N	Finite horizon
X_t	State at time t
$P(X_t X_{t-1})$	State transitions, typically Markovian
λ	Discount Factor $\in (0, 1]$
$r(X)$	Bounded reward function for continuing at state X
$g(X)$	Bounded reward function for stopping at state X

Table 3.1: Setup of finite horizon stopping problem

The objective is to find τ that maximizes

$$V(x) = \max_{\tau: \tau \leq N} \mathbb{E}[\lambda^\tau g(X_\tau) + \sum_{i=0}^{\tau-1} \lambda^i r(X_j) | X_0 = x] \quad (3.1)$$

The value function can be computed via backward induction by defining

$$\begin{aligned} J_N(x) &= g(x) \\ J_n(x) &= \max\{g(x), r(x) + \lambda \mathbb{E}_{P(y|x)}[J_{n+1}(y)]\}, \end{aligned} \tag{3.2}$$

$V(x) = J_0(x)$ and the optimal stopping time is

$$\tau = \min_{t \geq 0} J_t(X_t) = g(X_t) \tag{3.3}$$

For a derivation of the optimal stopping time, see Appendix C. The rest of this chapter covers how to formulate the stopping problem within an iteration of Bayesian optimization using the metabolic cost estimator. Let N be the maximum number of measurements allowed at a parameter evaluation, $\hat{x}_t \sim \mathcal{N}(\mu_{x_t}, \sigma_{x_t}^2)$ the cost estimate and associated variance for the current evaluation, and $\hat{x}^* \sim \mathcal{N}(\mu_{x^*}, \sigma_{x^*}^2)$ the cost estimate and variance for the best parameter setting found thus far. As there is an exploration phase \hat{x}^* will always be defined (Algorithm 1).

3.2 σ -scaled Offset

The σ -scaled offset model directly embeds \hat{x}_t and \hat{x}^* into the stopping problem. The best estimate of the difference in energetic costs is given by the following Gaussian distribution

$$\begin{aligned} \hat{x}_t - \hat{x}^* &\sim \mathcal{N}(\mu, \sigma^2) \\ \mu &= \mu_{x_t} - \mu_{x^*} \\ \sigma^2 &= \sigma_{x_t}^2 + \sigma_{x^*}^2 \end{aligned} \tag{3.4}$$

The stopping problem state is then the estimate difference, with a non-Markovian transition model of independent draws from the same Gaussian distribution. The reward function incentivizes continuing the lower x_t seems relative to x^* . In summary,

$$\begin{aligned}
X_t &= \mu \\
P(X_t|X_{t-1}) &= P(X_t) \sim \mathcal{N}(\mu, \sigma^2) \\
\lambda &= 1 \\
r(x) &= K\sigma - x \\
g(x) &= 0,
\end{aligned} \tag{3.5}$$

where K is a σ -scaled offset to provide some risk averseness to the estimate. The optimal stopping point for this formulation can be characterized as the first time $X_t > k\sigma$. As more measurements are taken and P_x decreases, σ^2 decreases the offset accordingly.

As shown in Section 2.3, underestimating P_w can cause the estimator to exhibit high volatility. Additionally, since a subsequent state covariance update $P_x(t+1)$ is bounded by P_w , a lower P_w will also cause σ^2 to be underestimated. With the σ -scaled offset model, underestimating the noisiness of observations could potentially cause promising parameter settings to stop measuring early as there is no fault tolerance for crossing the threshold.

3.3 Gittins Index

A more fault-tolerant model is drawn from literature related to the multi-armed bandit problem (MAB), which represents a sequential decision making problem where at any given time a player must select from different options (or arms) that then responds with a variable reward. Historically this has been used in a clinical context, where a physician must select from one of several different treatment options when presented a patient and receives binary rewards of either successes or failures (Sofia S. Villar and Wason, 2015). A stopping problem has also been described as a one-armed bandit problem (Gelman, 2004).

In our case, successes and failures can be based on μ, σ^2 using the Probability of Improvement (PI) metric

$$PI(\mu, \sigma^2) = \Phi\left(\frac{\mu}{\sigma}\right), \tag{3.6}$$

where Φ is the CDF for a standard normal distribution. A success can then be defined as $PI(\mu, \sigma^2) > T$ for some defined risk tolerance measure T . PI is inflated by a high σ^2 initially, and as more measurements are taken PI similarly decreases.

The state follows a Beta distribution where parameters α, β correspond to the count of successes and failures, and transitions follow the posterior of the Beta distribution. In summary,

$$X_t = (\alpha_t + \alpha_0, \beta_t + \beta_0)$$

$$P(X_{t+1}) = \begin{cases} (\alpha_t + \alpha_0 + 1, \beta_t + \beta_0) \\ \text{w.p. } \frac{\alpha_t + \alpha_0}{\alpha_t + \alpha_0 + \beta_t + \beta_0} \\ (\alpha_t + \alpha_0, \beta_t + \beta_0 + 1) \\ \text{w.p. } \frac{\beta_t + \beta_0}{\alpha_t + \alpha_0 + \beta_t + \beta_0} \end{cases} \quad (3.7)$$

$$r((\alpha_t + \alpha_0, \beta_t + \beta_0)) = \frac{\alpha_t + \alpha_0}{\alpha_t + \alpha_0 + \beta_t + \beta_0},$$

where α_0, β_0 are smoothing priors and α_t, β_t are successes and failures up to time t .

Gittins and Jones showed that an optimal policy could be constructed by calculating a value called the Gittins Index. Let $g(x) = K$ for some constant K , then the Gittins Index is defined as

$$\nu(x) = (1 - \lambda) \min_K \{J_0(x) = K\} \quad (3.8)$$

The Gittins Index is generally used for infinite horizon stopping problems, with $g(x) = \frac{\nu(x)}{1-\lambda}$ representing an infinite geometric sum to compensate for all future rewards. By setting $\lambda = 1 - \frac{1}{N}$, $\forall x \ 0 \leq \nu(x) \leq 1$.

The stopping condition for the one-armed bandit problem is equivalent to a two-armed bandit problem, where an imaginary second arm provides a constant reward V (Gelman, 2004). The optimal policy corresponds to playing the arm as long as its Gittins Index is above V . As T and V are correlated, one of the parameters can be fixed (such as $T = 0.5$)

while the other is tuned to a preferred risk tolerance for expected success rate.

3.4 Adaptive Thresholds

Having a constant risk threshold in either the σ -offset or Gittins model may be difficult to tune across subjects. Another approach is to use the exploration phase of Bayesian optimization to create a schedule for the thresholds adapted to the subject's measurements. Let M and Σ be $|\mathbb{E}| \times N$ matrices providing traces where M_{ij}, Σ_{ij} correspond to $\mu_{x_j}, \sigma_{x_j}^2$ for exploration point i and measurement j . For each exploration point, the \hat{x}^* distribution can be the final distribution at measurement N so as to have a sense of the magnitude of thresholds for comparing similar cost estimates. Algorithm 2 details the calculation of a threshold vector A .

3.5 Simulations

Simulations were run on four optimization functions. Measurements were given with a fixed noise corresponding to the standard deviation of the function. Both the σ -offset and Gittins models were then tested each with risk thresholds $T = [0, 0.25, 0.5]$. The case of $T = 0$ for the Gittins model is equivalent to a fixed measurement window and can be used as the point of comparison. A Kalman filter with the identity function for both F and H was used, essentially reconciling two Gaussian distributions, with $P_w = [\frac{\sigma^2}{10}, \sigma^2, 10\sigma^2]$.

```

Define  $|\mathbb{E}| \times N$  Matrix  $X$ 
Define  $N$ -Vector  $A$ 
Define Window  $W$ 
for  $i = 1$  to  $|\mathbb{E}|$ 
     $\alpha = \alpha_0, \beta = \beta_0$ 
    for  $j = 1$  to  $N$ 
         $\mu = M_{ij} - M_{iN}$ 
         $\sigma^2 = \Sigma_{ij} + \Sigma_{iN}$ 
        if  $Offset$ 
             $X_{ij} = \frac{\mu}{\sigma}$ 
        end
        if  $Gittins$ 
             $\alpha = \alpha + \mathbb{1}_{PI(\mu, \sigma^2) \geq T}$ 
             $\beta = \beta + \mathbb{1}_{PI(\mu, \sigma^2) < T}$ 
             $X_{ij} = v((\alpha, \beta))$ 
        end
    end
    end
for  $i = 1$  to  $N$ 
    if  $Offset$ 
         $A_i = \text{MAX}\{X_{rc} | 1 \leq r \leq N, i - W \leq c \leq i + W\}$ 
    end
    if  $Gittins$ 
         $A_i = \text{MIN}\{X_{rc} | 1 \leq r \leq N, i - W \leq c \leq i + W\}$ 
    end
end
Return  $A$ 

```

Algorithm 2: Determining threshold levels for either model based on subject's exploration data. With the σ -offset, a higher threshold is more risk averse, while with the Gittins model a lower is.

Function	Domain	Minimum	Mean	Std
Hartmann-6	$[0, 1]^6$	-3.322	-0.259	0.383
Ackley	$[-32.768, 32.768]^4$	0	20.882	1.027
Levy	$[-10, 10]^4$	0	42.544	27.939
Branin	$([-5, 10], [0, 15])$	0.398	54.452	51.129

Table 3.2: Optimization functions for simulations

Chapter 4

Results

4.1 Experimental Protocol

Optimization Parameters

An initial pilot was run varying 6 parameters

Peak Force	Maximum force in Newtons provided
Onset Timing	Start of assistance during the gait cycle
Peak Timing	Point of peak force provided during the gait cycle
Offset Timing	End of assistance during the gait cycle
Curvature 1	Force provided at midpoint of onset and peak
Curvature 2	Force provided at midpoint of peak and offset

Table 4.1: 6 parameters for providing a force profile

Hip-only Soft Exosuit

The textile components of the hip-only soft exosuit consist of a short spandex base layer, a waist belt, and two thigh braces as described in (Lee *et al.*). Two IMUs (MTi-3 AHRS, Xsens Technologies B.V., Enschede, Netherlands) mounted on the anterior part of the thigh measure the orientation and angular velocity of thigh segments which are used for gait cycle estimation in real-time (Ding *et al.*, 2016). The anchoring points of the Bowden cable are at the bottom left and right of the waist belt as well as at the middle center of the thigh braces from the posterior view. Two load cells (LSB200, Futek Advanced Sensor Technology Inc., CA, USA) are integrated in the aluminum attachment piece of the anchoring point to measure the cable force. When the actuator pulls the inner cable, the soft exosuit generates a hip extension torque by shortening the distance between two anchoring points.

Actuation System

The two DOF actuators in the off-board system are used to deliver hip extension assistance to both legs. Each actuator consists of a customized brushless motor (Allied Motion, Colorado, USA), a 9.25:1 spiroid gear set (ITW Heartland, MN, USA) and a 45 mm radius pulley. The pulley groove is designed to be able to wrap the inner Bowden cable 1.5 times around the pulley, allowing 420 mm of cable travel (Lee *et al.*). A 360 counts/rev incremental encoder (AS5134-ZSST, ams AG, Premstaetten, Austria) is mounted on the customized motor to measure its position and velocity. The Bowden cable sheath of the actuator side connects to the pulley cover and inner cable attaches to the pulley. When the motor rotates, the actuator can either pull in the inner cable to generate a force or push the cable out so it can go slack.

Control System Architecture

The electronics hardware has a three-layer configuration for the control system architecture: real-time target machine (top layer), microprocessor (middle layer), and servomotor driver (bottom layer). In the top layer, the Speedgoat real-time target machine runs a Simulink model in a host laptop. A PCI interface card (CAN-AC PCI, Softing AG, Haar, Germany) for

CAN communication is installed on the target machine to acquire sensor signals and send the command to the servomotor driver through the microprocessor. The microprocessor (Due, Arudino, Ivrea, Italy) in the middle layer acts as a signal hub between target machine and servomotor driver while protecting the system from undesired behavior of the actuator due to anomalous errors from the target machine. In the bottom layer, Gold Twitter (Elmo Motion Control Ltd, Israel) with 55V maximum supply voltage and 60 A peak current is selected as the current servomotor driver. It tracks the current command from the microprocessor to drive the actuator. The CAN communication between layers closes the control loop at 1kHz loop rate (Lee *et al.*).

Another laptop collects the metabolic data, runs an optimization algorithm, and sends the assistance profile parameters that will be explored in the next condition to the host laptop. Ethernet communication is used between a real-time target machine, a host laptop, and the second laptop. Based on the profile parameters calculated by the algorithm, the host laptop sends the current command to the servomotor drive to deliver assistance to the subject.

4.2 Experimental Subjects

Two male subjects (S1: 27 yrs, 74 kg, 177 cm; S2: 48 yrs, 85 kg, 178 cm) participated in this preliminary study. The subjects walked on the treadmill at 1.25 m/s under four different conditions: Normal walking without Exosuit (N), Exosuit-off (OFF), Fixed Exosuit Assistance (FIX) and Optimal Exosuit Assistance (OPT). During FIX condition, the force profiles assisting hip extension were based on the previous study of (Ding *et al.*, 2016), whereas force profiles in OPT condition were determined through a two-part procedure (8 exploration points, 5 minute break, then 40 minute continuous optimization) which was performed before walking test conditions. Metabolic cost of walking across different conditions was measured using a portable gas analysis system (K4b2, Cosmed, Roma, Italy).

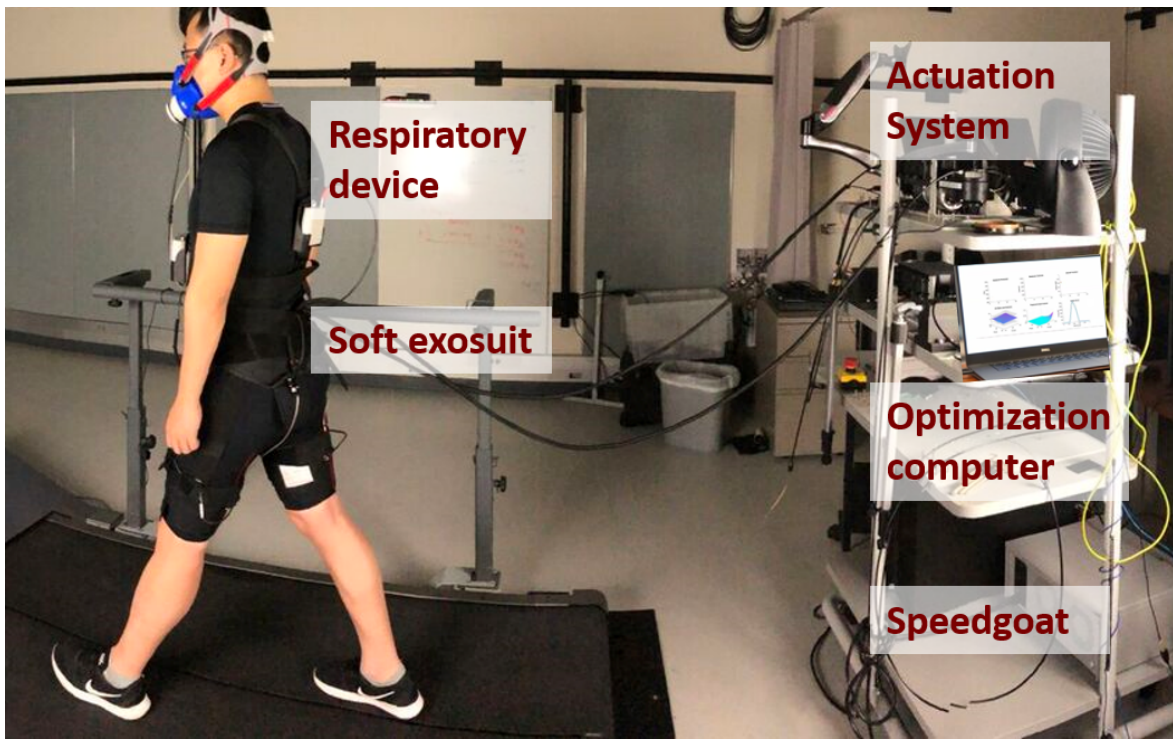


Figure 4.1: Experimental setup. Assistance parameters for the soft exosuit were optimized on-line. Respiratory device measured respiratory rate to estimate metabolic cost for a given condition with a covariance. In the optimization computer, the Gittins process determined when to stop sampling and Bayesian optimization was used to select a next parameter set. The parameters were sent to the real-time computer (speedgoat) to generate a force trajectory. Then, the actuator provided a force to a subject through a bowden cables.

4.3 Results

Two human trials with the same subjects from a previous study were conducted as a comparison. The Gittins method was used with a relatively risk averse $K = 0.35$ to account for the possibility of a very low signal-to-noise ratio, as well as the practical consideration of parameters requiring time to fully propagate to the suit. A summary of the metabolic reduction can be found in Table 4.2 with figures for the optimized force assistance in Figure 4.3. The soft exosuit followed desired trajectory within 5% error, relative to the peak force.

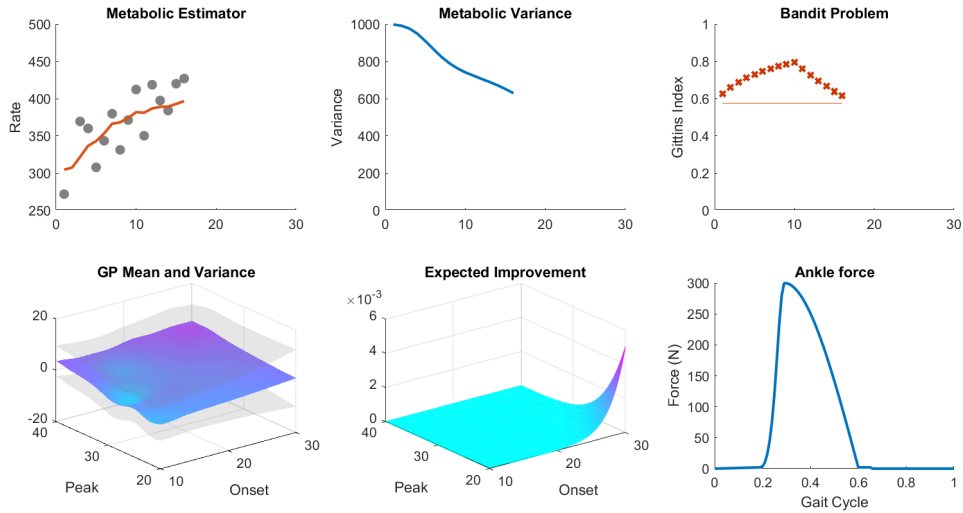


Figure 4.2: Diagram of Bandit Process

Subj	OPT	FIX	OPT Peak F	FIX Peak F
1	35%	29%	223N	247N
2	7%	-4%	174N	230N

Table 4.2: Subject Trial Summary

4.4 Conclusions

A new metabolic estimator based off the Unscented Kalman Filter algorithm was designed to enable early stopping for a parameter evaluation. The estimator has shown the ability to track the instantaneous metabolic rate online with varying amounts of data, but is sensitive to the parameterization of it's covariance matrices. Two methods were developed for early stopping: a simple σ -offset threshold strategy and a bandit process strategy based off the Gittins Index. Depending on the noisiness of the estimator, the bandit process provides a higher fault tolerance for noisy observations. Two trials were then conducted using the Gittins algorithm to optimize over six hip parameters and we found comparable metabolic reduction to a previous study with the same subjects. In the previous study ample time was spent isolating the parameters individually to find the two with high variability (peak and offset timing). While the optimization period for a trial is slightly longer, we were

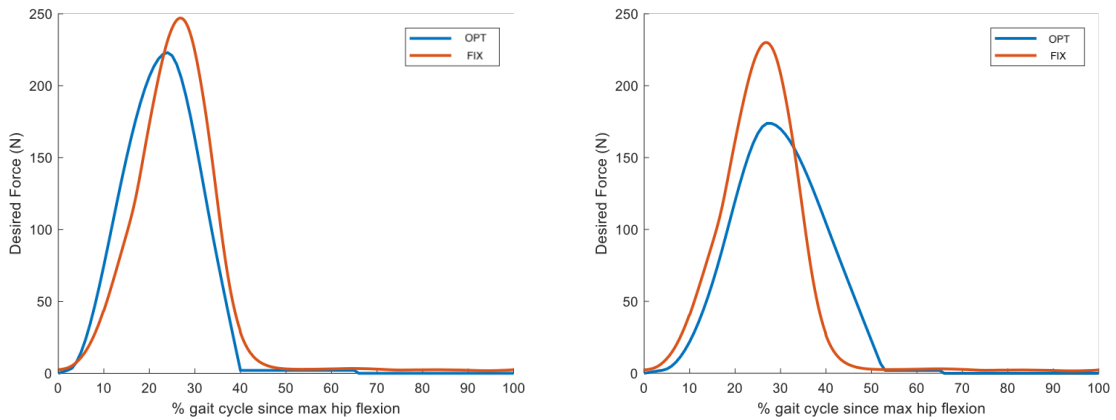


Figure 4.3: Force profiles of the two subjects

able to find similar results without the need for an extensive pre-trial exploration phase. Interestingly, we also found a lower peak force to provide similar metabolic reduction in each of the two subjects. Having a lower peak force could provide two benefits: lower battery requirements on the suit and more importantly reduced strain on the harness and subsequent discomfort to the user. Future work in this area can focus on tuning the estimator's covariance matrices with exploration phase data and testing more subjects with both models. In particular, an area of interest would be using the algorithm in multi-joint optimization (Lee *et al.*, 2018).

References

- ASSAEL, J.-A. M., WANG, Z., SHAHRIARI, B. and DE FREITAS, N. (2014). Heteroscedastic treed bayesian optimisation.
- BARBER, D., CEMGIL, A. and CHIAPPA, S. (2011). *Bayesian Time Series Models*. Bayesian Time Series Models, Cambridge University Press.
- BROCHU, E., HOFFMAN, M. W. and DE FREITAS, N. (2010). Portfolio allocation for bayesian optimization.
- BROCHU, V. M. C., ERIC and DE FREITAS, N. (2010). A tutorial on bayesian optimization of expensive cost functions, with application to active user modeling and hierarchical reinforcement learning. *Technical Report*, pp. TR-2009-23.
- BROCKWAY, J. M. (1987). Derivation of formulae used to calculate energy expenditure in man. **41C**, 463–471.
- CAPUTO, J. M., ADAMCZYK, P. G. and COLLINS, S. H. (2015). Informing ankle-foot prosthesis prescription through haptic emulation of candidate devices. pp. 6445 – 6450.
- and COLLINS, S. H. (2014). A universal ankle-foot prosthesis emulator for experiments during human locomotion. *JBME*, **136**, 035002.
- COLLINS, S. H., WIGGIN, M. B. and SAWICKI, G. S. (2015). Reducing the energy cost of human walking using an unpowered exoskeleton. *Nature*, **522**, 212–215.
- DING, Y., GALIANA, I., ASBECK, A. T., ROSSI, S. M. M. D., BAE, J., SANTOS, T. R. T., DE ARAUJO, V. L., LEE, S., HOLT, K. G. and WALSH, C. (2017). Biomechanical and physiological evaluation of multi-joint assistance with soft exosuits. **25** (2), 119–130.
- , KIM, M., KUINDERSMA, S. and WALSH, C. J. (2018). Human-in-the-loop optimization of hip assistance with a soft exosuit during walking. *Science Robotics*, **3** (15).
- , PANIZZOLO, F. A., SIVIY, C., MALCOLM, P., GALIANA, I., HOLT, K. G. and WALSH, C. J. (2016). Effect of timing of hip extension assistance during loaded walking with a soft exosuit. *JNER*, **13** (1), 87.
- FELT, W., SELINGER, J. C., DONELAN, J. M. and REMY, C. D. (2015). "Body-In-The-Loop": Optimizing Device Parameters Using Measures of Instantaneous Energetic Cost. *PloS one*, **10** (8), e0135342.

- GELMAN, A. (2004). *Bayesian Data Analysis*. Texts in statistical science, Chapman & Hall/CRC.
- GONZÁLEZ, J., OSBORNE, M. and LAWRENCE, N. D. (2015). Glasses: Relieving the myopia of bayesian optimisation.
- JARNO VANHATALO, J. H. P. J. V. T., JAAKKO RIIHIMÄKI and VEHTARI, A. (2013). Gpstuff: Bayesian modeling with gaussian processes. *Journal of Machine Learning Research*, **14**, 1175–1179.
- JULIER, S. J. (1997). A new extension of the kalman filter to nonlinear systems. *Int. Symp. Aerospace/Defense Sensing, Simul. and Controls*, **3**.
- JYLÄNKI, P., VANHATALO, J. and VEHTARI, A. (2011). Robust gaussian process regression with a student-t likelihood. *J. Mach. Learn. Res.*, **12**, 3227–3257.
- KIM, M. and COLLINS, S. H. (2015). Once-per-step control of ankle-foot prosthesis push-off work reduces effort associated with balance during walking. **12** (1), 43.
- and — (2017). Step-to-step ankle inversion/eversion torque modulation can reduce effort associated with balance. *Frontiers in neurorobotics*, **11**, 62.
- , DING, Y., MALCOLM, P., SPEECKAERT, J., SIVIY, C. J., WALSH, C. J. and KUINDERSMA, S. (2017). Human-in-the-loop bayesian optimization of wearable device parameters. *PloS one*, **12** (9), e0184054.
- KOLLER, J. R., GATES, D. H., FERRIS, D. P. and REMY, C. D. (2016). 'body-in-the-loop' optimization of assistive robotic devices: A validation study. In *Robotics: Science and Systems*.
- LAM, R., WILLCOX, K. and WOLPERT, D. H. (2016). Bayesian optimization with a finite budget: An approximate dynamic programming approach. In D. D. Lee, M. Sugiyama, U. V. Luxburg, I. Guyon and R. Garnett (eds.), *Advances in Neural Information Processing Systems* 29, Curran Associates, Inc., pp. 883–891.
- LEE, G., DING, Y., BUJANDA, I. G., KARAVAS, N., ZHOU, Y. M. and WALSH, C. J. (). Improved assistive profile tracking of soft exosuits for walking and jogging with off-board actuation.
- LEE, S., CREA, S., MALCOLM, P., GALIANA, I., ASBECK, A. and WALSH, C. (2016). Controlling negative and positive power at the ankle with a soft exosuit. pp. 3509–3515.
- , KARAVAS, N., QUINLIVAN, B., RYAN, D., PERRY, D., ECKERT-ERDHEIM, A., MURPHY, P., GREENBERG GOLDY, T., MENARD, N., ATHANASSIU, M., KIM, J., LEE, G., GALIANA, I. and WALSH, C. (2018). Autonomous multi-joint soft exosuit for assistance with walking overground. In *IEEE International Conference on Robotics and Automation (ICRA)*, Brisbane, Australia, May 21-25.
- LIZOTTE, D. J. (2008). *Practical Bayesian Optimization*. Ph.D. thesis, Edmonton, Alta., Canada, aAINR46365.
- MAHENDRAN, N., WANG, Z., HAMZE, F. and FREITAS, N. D. (2012). Adaptive mcmc with bayesian optimization. In N. D. Lawrence and M. Girolami (eds.), *Proceedings of the Fifteenth International Conference on Artificial Intelligence and Statistics*, La Palma, Canary Islands: PMLR, *Proceedings of Machine Learning Research*, vol. 22, pp. 751–760.

- MALCOLM, P., DERAVE, W., GALLE, S. and DE CLERCQ, D. (2013). A simple exoskeleton that assists plantarflexion can reduce the metabolic cost of human walking. *PLoS one*, **8** (2), e56137.
- MOONEY, L. M. and HERR., H. M. (2016). Biomechanical walking mechanisms underlying the metabolic reduction caused by an autonomous exoskeleton. **13** (1), 4.
- NOGUEIRA, J., MARTINEZ-CANTIN, R., BERNARDINO, A. and JAMONE, L. (2016). Unscented bayesian optimization for safe robot grasping.
- PANIZZOLO, F. A., GALIANA, I., ASBECK, A. T., SIVIY, C., SCHMIDT, K., HOLT, K. G. and WALSH, C. J. (2016a). A biologically-inspired multi-joint soft exosuit that can reduce the energy cost of loaded walking. **13** (1), 43.
- , —, —, —, — and WALSH., C. J. (2016b). A biologically-inspired multi-joint soft exosuit that can reduce the energy cost of loaded walking. *JNER*, **13**, 1–13.
- QUESADA, R. E., CAPUTO, J. M. and COLLINS, S. H. (2016). Increasing ankle push-off work with a powered prosthesis does not necessarily reduce metabolic rate for transtibial amputees. **49** (14), 3452–3459.
- QUINLIVAN, B., LEE, S., MALCOLM, P., ROSSI, D., GRIMMER, M., SIVIY, C., KARAVAS, N., WAGNER, D., ASBECK, A., GALIANA, I. and WALSH, C. (2017). Assistance magnitude versus metabolic cost reductions for a tethered multiarticular soft exosuit. *Science Robotics*, **2** (2), eaah4416.
- RASMUSSEN, C. E. (2006). Gaussian processes for machine learning.
- RUE, H., MARTINO, S. and CHOPIN, N. (2009). Approximate Bayesian inference for latent Gaussian models by using integrated nested Laplace approximations. *Journal of the Royal Statistical Society: Series B (Statistical Methodology)*, **71** (2), 319–392.
- SELINGER, J. C. and DONELAN., J. M. (2014). Estimating instantaneous energetic cost during non-steady-state gait. **117** (11), 1406–1415.
- SNOEK, J., LAROCHELLE, H. and ADAMS, R. P. (2012). Practical bayesian optimization of machine learning algorithms. In F. Pereira, C. J. C. Burges, L. Bottou and K. Q. Weinberger (eds.), *Advances in Neural Information Processing Systems 25*, Curran Associates, Inc., pp. 2951–2959.
- SOFIA S. VILLAR, J. B. and WASON, J. (2015). Multi-armed bandit models for the optimal design of clinical trials: Benefits and challenges. *Statistical Science*, **30** (2), 199–215.
- VANHATALO, J., JYLÄNKI, P. and VEHTARI, A. (2009). Gaussian process regression with student-t likelihood. In Y. Bengio, D. Schuurmans, J. D. Lafferty, C. K. I. Williams and A. Culotta (eds.), *Advances in Neural Information Processing Systems 22*, Curran Associates, Inc., pp. 1910–1918.
- WAN, E. A. and MERWE, R. V. D. (2000). The unscented kalman filter for nonlinear estimation. pp. 153–158.

ZHANG, J., FIERS, P., WITTE, K. A., JACKSON, R. W., POGGENSEE, K. L., ATKESON, C. G. and COLLINS, S. H. (2017). Human-in-the-loop optimization of exoskeleton assistance during walking. *Science*, **356** (6344), 1280–1284.

Appendix A

Bayesian Optimization

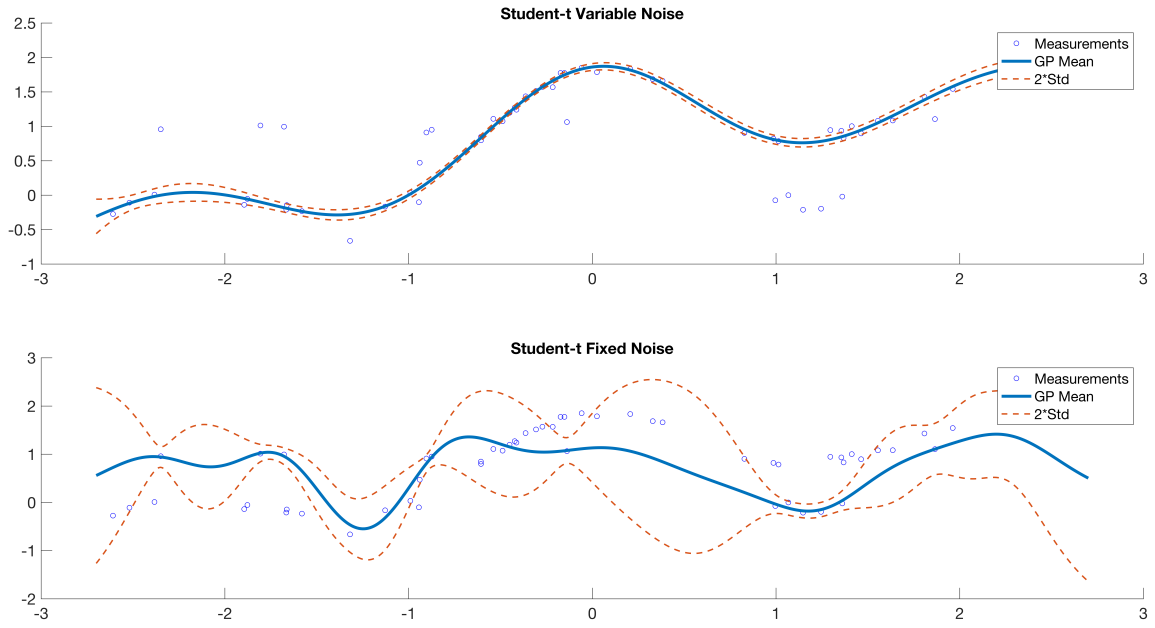
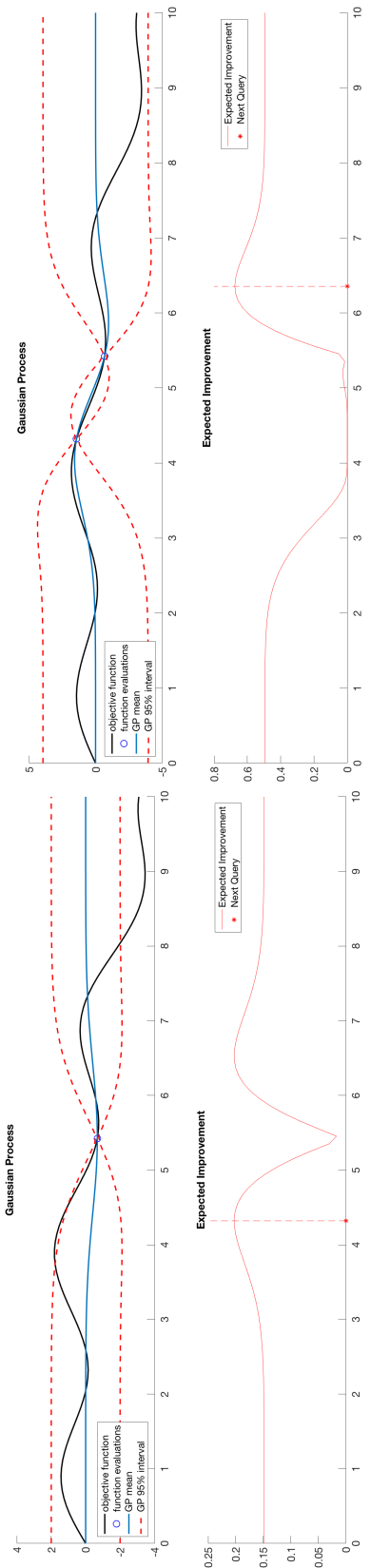
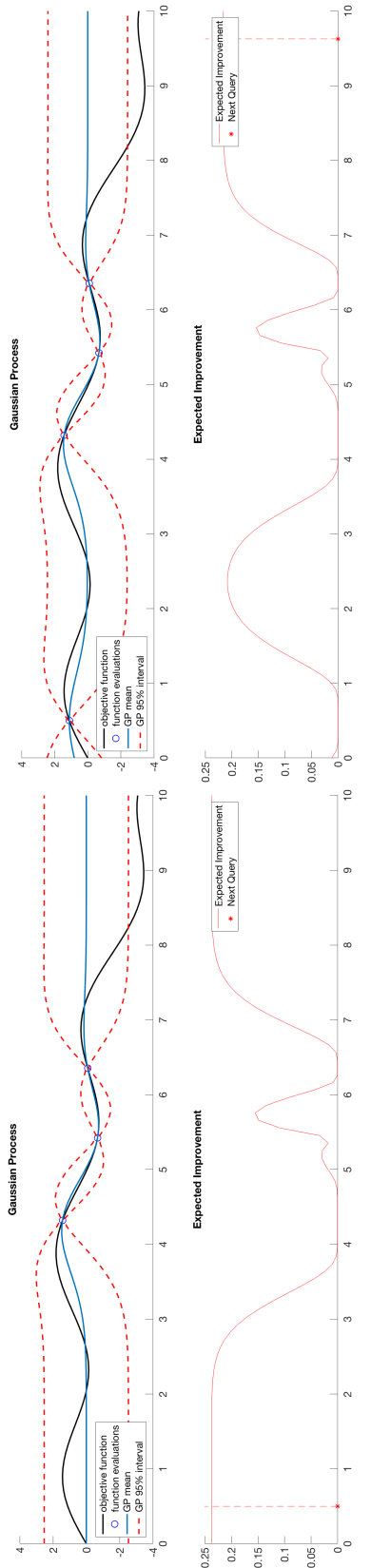


Figure A.1: Demonstration of the effect of fixing measurement noise for each data point. Using the same data from Figure 1.2, the top graph shows the same MCMC graph that infers the noise hyperparameters with the highest likelihood. In the bottom graph, the noise parameters are fixed and inversely proportional to the true accuracy - in effect telling the GP that the outliers are the correct values. This may arise in situations where a minimum is found (measured for the full duration, resulting variance is relatively low) and many nearby points are subsequently sampled and stopped early (resulting variances are very high).



(a) Iterations 1 and 2



(b) Iterations 3 and 4

Figure A.2: Four Iterations of Bayesian Optimization

Appendix B

Unscented Kalman Filter¹

The unscented transformation selects a representative set of points (sigma points) with associated weights to propagate through a nonlinear function. More formally, given an N -dimensional random variable x with mean \bar{x} and covariance P_x we calculate the following sigma vectors

$$\begin{aligned}\chi_0 &= \bar{x} \\ \chi_i &= \bar{x} + (\sqrt{(N + \lambda)P_x})_i & i = 1, \dots, N \\ \chi_i &= \bar{x} - (\sqrt{(N + \lambda)P_x})_{i-N} & i = N + 1, \dots, 2N \\ W_0^{(m)} &= \lambda / (N + \lambda) \\ W_0^{(c)} &= \lambda / (N + \lambda) + (1 - \alpha^2 + \beta) \\ W_i^m = W_i^c &= 1 / \{(2(N + \lambda))\} & i = 1, \dots, 2N,\end{aligned}\tag{B.1}$$

where $(\sqrt{(N + \lambda)P_x})_i$ represents the i th row of the matrix square root, $\lambda = \alpha^2(N + \kappa) - N$, and α , κ , and β are scaling parameters. For a given nonlinear function $y = g(x)$, an estimate for the mean and covariance are then

$$\begin{aligned}\bar{y} &\approx \sum_{i=0}^{2N} W_i^{(m)} g(\chi_i) \\ P_y &\approx \sum_{i=0}^{2N} W_i^{(c)} (g(\chi_i) - \bar{y})(g(\chi_i) - \bar{y})^T\end{aligned}\tag{B.2}$$

¹Wan and Merwe (2000)

Accurate to the second order, the Unscented Kalman Filter incorporates this transformation in its F and H functions as follows:

Initial State Estimate and Covariance $\hat{x}(0), P_x(0)$

Define Augmented State $x^a = [x^T \quad v^T \quad w^T]^T$

Define Augmented Sigma Points $\chi^a = [(\chi^x)^T \quad (\chi^v)^T \quad (\chi^w)^T]^T$

Initial Augmented State Estimate $\hat{x}^a(0) = [\hat{x}(0)^T \quad 0 \quad 0]^T$

Initial Augmented Covariance $P^a(0) = \begin{bmatrix} P_x(0) & 0 & 0 \\ 0 & P_v & 0 \\ 0 & 0 & P_w \end{bmatrix}$

for $t = 1$ **to** T

Using B.1 Calculate Sigma Points $\chi^a(t)$ And Weights $W^{(m)}, W^{(c)}$

Time Update:

$$\chi_i^x(t|t-1) = F(\chi_i^x(t-1), \chi_i^v(t-1), t-1)$$

$$\hat{x}(t|t-1) = \sum_{i=0}^{2N} W_i^{(m)} \chi_i^x(t|t-1)$$

$$P_x(t|t-1) = \sum_{i=1}^{2N} W_i^{(c)} \{ \chi_i^x(t|t-1) - \hat{x}(t|t-1) \} \{ \chi_i^x(t|t-1) - \hat{x}(t|t-1) \}^T$$

$$\mathbb{Z}_i(t|t-1) = H(\chi_i^x(t|t-1), \chi_i^v(t|t-1), t-1)$$

$$\hat{z}(t|t-1) = \sum_{i=1}^{2N} W_i^{(m)} \mathbb{Z}_i(t|t-1)$$

Measurement Update:

$$P_y(t|t-1) = \sum_{i=1}^{2N} W_i^{(c)} \{ \mathbb{Z}_i(t|t-1) - \hat{z}(t|t-1) \} \{ \mathbb{Z}_i(t|t-1) - \hat{z}(t|t-1) \}^T$$

$$P_{xy}(t|t-1) = \sum_{i=1}^{2N} W_i^{(c)} \{ \chi_i^x(t|t-1) - \hat{x}(t|t-1) \} \{ \chi_i^x(t|t-1) - \hat{x}(t|t-1) \}^T$$

$$K = P_{xy}(t|t-1) P_y^{-1}(t|t-1)$$

$$\hat{x}(t) = \hat{x}(t|t-1) + K(z(t) - \hat{z}(t|t-1))$$

$$P_x(t) = P_x(t|t-1) - K P_y(t|t-1) K^T$$

end

Appendix C

Optimal Stopping Time Derivation

Define the process

$$Z_n = \sum_{i=0}^{n-1} \lambda^i r(X_i) + \lambda^n J_n(X_n)$$

Then, we have

$$\begin{aligned} \mathbb{E}[Z_{n+1}|X_n, X_{n-1}, \dots, X_0] &= \sum_{i=0}^n \lambda^i r(X_i) + \lambda^{n+1} \mathbb{E}[J_{n+1}(X_{n+1})|X_n] \\ &= \sum_{i=0}^{n-1} \lambda^i r(X_i) + \lambda^n (r(X_n) + \lambda \mathbb{E}[J_{n+1}(X_{n+1})|X_n]) \\ &\leq \sum_{i=0}^{n-1} \lambda^i r(X_i) + \lambda^n J_n(X_n) = Z_n \end{aligned}$$

Since by definition $J_n(x) \geq g(x)$, we have

$$\mathbb{E}\left[\sum_{i=0}^{\tau-1} \lambda^i r(X_i) + \lambda^\tau g(X_\tau)\right] \leq \mathbb{E}[Z_\tau] \leq \mathbb{E}[Z_0] = J_0(X_0)$$

for any stopping time $\tau \geq 0$.

We now prove that $J_0(X_0)$ is exactly equal to $\mathbb{E}[Z_{\tau^*}]$ for optimal stopping time τ^* .

Consider the following for $0 \leq n < N$

$$\begin{aligned}
& \mathbb{E}[Z_{\min(\tau^*, n+1)} | X_n, X_{n-1}, \dots, X_0] \\
&= 1_{\{\tau^* \leq n\}} Z_{\tau^*} + 1_{\{\tau^* > n\}} \mathbb{E}[Z_{n+1} | X_n, X_{n-1}, \dots, X_0] \\
&= 1_{\{\tau^* \leq n\}} Z_{\tau^*} + 1_{\{\tau^* > n\}} \left(\sum_{i=0}^n \lambda^i r(X_i) + \lambda^{n+1} \mathbb{E}[J_{n+1}(X_{n+1}) | X_n] \right) \\
&= 1_{\{\tau^* \leq n\}} Z_{\tau^*} + 1_{\{\tau^* > n\}} \left(\sum_{i=0}^{n-1} \lambda^i r(X_i) + \lambda^n J_n(X_n) \right) \quad (\tau^* > n \leftrightarrow J_n(X_n) = r(x) + \lambda \mathbb{E}[J_{n+1}(X_{n+1})]) \\
&= 1_{\{\tau^* \leq n\}} Z_{\tau^*} + 1_{\{\tau^* > n\}} Z_n \\
&= Z_{\min(\tau^*, n)}
\end{aligned}$$

Then, it follows that

$$\begin{aligned}
J_0(X_0) &= \mathbb{E}[Z_0] = \mathbb{E}[Z_{\min(\tau^*, 0)}] = \dots = \mathbb{E}[Z_{\min(\tau^*, N)}] = \mathbb{E}[Z_{\tau^*}] \\
&= \mathbb{E}\left[\sum_{i=0}^{\tau^*-1} \lambda^i r(X_i) + \lambda^{\tau^*} J_{\tau^*}(X_{\tau^*})\right] = \mathbb{E}\left[\sum_{i=0}^{\tau^*-1} \lambda^i r(X_i) + \lambda^{\tau^*} g(X_{\tau^*})\right]
\end{aligned}$$

and $J_{\tau^*}(X_{\tau^*}) = g(X_{\tau^*})$ at τ^* .